**ADVANCED
SCIENCE NEWS**
www.advancedsciencenews.com

**ADVANCED
HEALTHCARE
MATERIALS**
www.advhealthmat.de

FULL PAPER

Green Synthesis of Sub-10 nm Gadolinium-Based Nanoparticles for Sparkling Kidneys, Tumor, and Angiogenesis of Tumor-Bearing Mice in Magnetic Resonance Imaging

Bingbo Zhang,* Weitao Yang, Jiani Yu, Weisheng Guo, Jun Wang, Shiyuan Liu, Yi Xiao,* and Donglu Shi*

Gadolinium (Gd)-based nanoparticles are known for their high potential in magnetic resonance imaging (MRI). However, further MRI applications of these nanoparticles are hampered by their relatively large sizes resulting in poor organ/tumor targeting. In this study, ultrafine sub-10 nm and biocompatible Gd-based nanoparticles are synthesized in a bioinspired, environmentally benign, and straightforward fashion. This novel green synthetic strategy is developed for growing dextran-coated Gd-based nanoparticles (GdNPs@Dex). The as-prepared GdNPs@Dex is not only biocompatible but also stable with a sub-10 nm size. It exhibits higher longitudinal and transverse relaxivities in water (r_1 and r_2 values of 5.43 and 7.502 s^{-1} × 10^{-3} M^{-1} of Gd^{3+}, respectively) than those measured for Gd–DTPA solution (r_1 and r_2 values of 3.42 and 3.86 s^{-1} × 10^{-3} M^{-1} of Gd^{3+}, respectively). In vivo dynamic T_1-weighted MRI in tumor-bearing mice shows GdNPs@Dex can selectively target kidneys and tumor, in addition to liver and spleen. GdNPs@Dex is found particularly capable for determining the tumor boundary with clearly enhanced tumor angiogenesis. GdNPs@Dex is also found cleared from body gradually mainly via hepatobiliary and renal processing with no obvious systemic toxicity. With this green synthesis strategy, the sub-10 nm GdNPs@Dex presents promising potentials for translational biomedical imaging applications.

1. Introduction

Contrast-enhanced magnetic resonance imaging (MRI) has been extensively medically employed for its high signal-to-noise ratio and refined resolution, utilized with the aid of contrast agents.[1] Gd-DTPA, the so-called Magnevist, is one of the most frequently used contrast agents in clinic settings.[2] Although stable in its molecular structure, it is limited by poor relaxivity, specificity, and retention time in blood stream.[3] These barriers significantly hinder its applications in target-specific imaging and dynamic MRI. There is, therefore, a great need to search for the biocompatible contrast agents that exhibit high sensitivity and specificity for targeting desired organs or tumors with a large imaging time-window.

Nanoparticle-based contrast agents are particularly promising candidates for addressing these critical issues.[4,5] Unique properties have been observed from the newly discovered nanomaterials including

Prof. B. Zhang, J. Yu, Dr. J. Wang
Institute of Photomedicine
Shanghai Skin Disease Hospital
The Institute for Biomedical Engineering and Nano Science
Tongji University School of Medicine
Shanghai 200443, China
E-mail: bingbozhang@tongji.edu.cn
Dr. W. Yang
School of Materials Science and Engineering
School of Life Science
Tianjin Engineering Center of Micro-Nano Biomaterials
and Detection-Treatment Technology
Tianjin University
Tianjin 300072, China
Dr. W. Guo
CAS Key Laboratory for Biological Effects of
Nanomaterials and Nanosafety
National Center for Nanoscience and Technology
No. 11 Beiyitiao, Zhongguancun, Beijing 100190, China

Prof. S. Liu, Dr. Y. Xiao
Department of Radiology
Changzheng Hospital
The Second Military Medical University
Shanghai 200003, China
E-mail: xiaoyi@188.com
Prof. D. Shi
The Institute for Translational Nanomedicine
Shanghai East Hospital
The Institute for Biomedical Engineering and Nano Science
Tongji University School of Medicine
Shanghai 200092, P. R. China
E-mail: donglushi@tongji.edu.cn
Prof. D. Shi
Department of Mechanical and Materials Engineering
College of Engineering and Applied Science
University of Cincinnati
Cincinnati, OH 45221-0072, USA

ADVANCED
HEALTHCARE
MATERIALS

www.advhealthmat.de

ADVANCED
SCIENCE NEWS

www.advancedsciencenews.com

metals, semiconductors, ceramics, and polymers for biomedical imaging.[6–9] The relaxivities of nanoparticle-based contrast agents can be improved over their small molecular counterparts.[8,10] And the free surface area on the nanosized contrast agents is readily available for conjugating with antibodies, peptides, aptamers, and drugs, which can enhance their targeting capabilities and theranostic functionalities.[11] The nanosized contrast agents are advantageously characterized by prolonged circulation time in vivo, and enhanced delivery to the target area.[12]

Two major nano-based MRI contrast agents have been developed, namely, superparamagnetic iron oxide (SPIO) nanoparticles and Gd-based nanoparticles.[9,10,13,14] The SPIOs are reported to have high r_2/r_1 ratios, usually characterized as the negative contrast agents for liver disease MRI. Due to their relatively large sizes, SPIOs can be easily captured by macrophagocyte in liver.[10] The blooming effect of SPIO in T_2-weighted MRI has been observed to amplify the signals due to affected protons at the distant sites. This effect often exaggerates the size of labeled area and blurs the image, making it difficult to distinguish suspected lesions from the adjacent normal tissues.[15] Gd-based nanoparticles with low r_2/r_1 ratios, as T_1-positive contrast agents, exhibit much improved brightening performance of MRI and tissue/lesion differentiation.

However, the current synthesis techniques for developing Gd-based nanoparticles are largely hindered in part by high-energy consumption (high temperatures), stringent conditions (pH values, ionic strengths, and pressure), and low reproducibility and yield.[16] There is an increasing need to develop eco-friendly and effective methods for producing ultrafine Gd-based nanoparticles for efficient targeting, especially for kidney imaging. Relative large sized Gd-based nanoparticles can easily induce reticuloendothelial system (RES) captures, resulting in skimpy kidney, tumor accumulation, and poor tumor margin enhancement.

In this work, a unique approach was developed to synthesize the inorganic–organic Gd-based hybrid nanoparticles via dextran-assisted green chemistry. The Gd-based hybrid nanoparticles were derived from a suspension of gadolinium chloride hexahydrate, dextran, and ammonium hydroxide in a straightforward, environmentally benign, one-pot, and reproducible synthetic route at low temperature. The synthesis is similar to biomineralization of organisms in nature: sequestering and interacting with inorganic ions, followed by providing scaffolds for the minerals formed.[14,17] The dextran molecules sequester the Gd ions and entrap them upon adding Gd^{3+} ions into the aqueous dextran solution. The entrapped ions to form Gd-based nanoparticles in situ are then activated by adjusting the pH. This progressive reaction is assisted by the scaffold ability of dextran molecules and slightly heated for crystallization.

The method developed in this study is simple, reproducible, and environmentally benign. The resulting GdNPs@Dex are sub-10 nm in hydrodynamic diameter and exhibiting excellent imaging performance on the whole body level, sparkling the kidneys, liver, spleen, tumor, and tumor angiogenesis at the edge.

2. Results and Discussion

2.1. Physicochemical Properties of GdNPs@Dex

A green chemistry was employed to synthesize Gd-based nanoparticles assisted by the FDA-approved dextran at low temperature for MR imaging on the whole body level, sparkling the kidneys, liver, spleen, tumor, and tumor angiogenesis at the edge, as shown in **Scheme 1**.

We screened key parameters including the feeding ratios of dextran to GdCl$_3$·6H$_2$O (i.e., 150 mg:40 mg; 75 mg:40 mg; and 37.5 mg:40 mg) and reaction temperatures (25, 37, and 80 °C) in the synthesis of GdNPs@Dex. It was found that the reaction solutions in the samples of 75 and 37.5 mg of dextran were turbid, while solution was optically clear in the sample of 150 mg of dextran, indicating the dextran should be sufficient for the formation of nanoparticles (Figure S1, Supporting
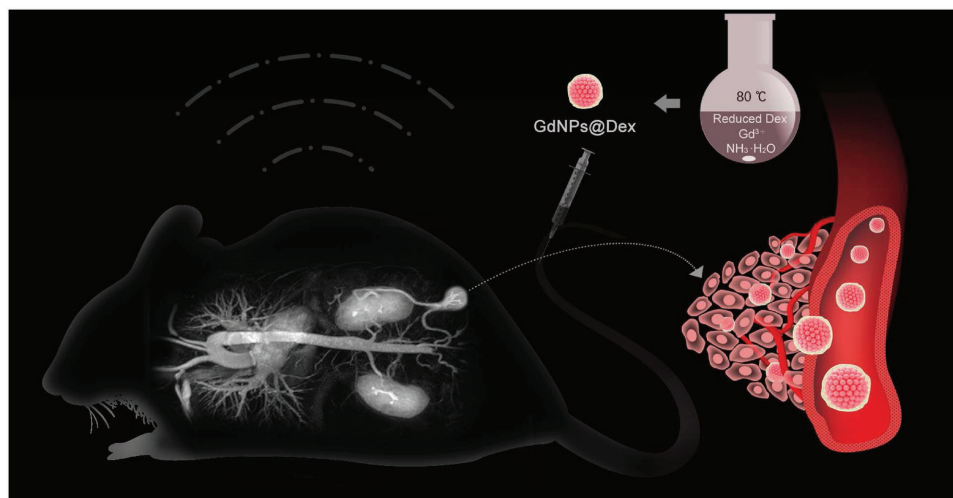

Scheme 1. Illustration of the one-pot and facile synthesis of GdNPs@Dex and its MR imaging performance on the whole body, plus tumor and tumor angiogenesis.

Information). Upon determining the optimal feeding ratio, the reaction temperature was further investigated. It suggests no obvious difference on hydrodynamic diameters of the resulting samples synthesized at 25, 37, and 80 °C (Figure S2, Supporting Information). However, relaxation rate test results show reaction at relatively higher temperature can produce higher r_1 and r_2 of GdNPs@Dex (Figure S3, Supporting Information). This temperature-dependent relaxation improvement is most likely associated to the high conversion ratio of Gd^{3+} ions to GdNPs@Dex at high temperature. At lower temperatures, most of Gd^{3+} ions were lost in crystallization, which reduces the effective concentrations of GdNPs@Dex in solution. Therefore, the feeding ratio of dextran to $GdCl_3 \cdot 6H_2O$ is determined at 150 mg:40 mg and the reaction temperature is set at 80 °C for GdNPs@Dex synthesis.

Dextran is an abundant, inexpensive polymer that consists solely of α-D-glucopyranosyl monomers. Dextran has a large number of hydroxyl groups that provide chelation and hydrogen-bonding interactions with added Gd^{3+} ions, forming polysaccharide-Gd^{3+} intermediates. Particularly, the macromolecular structure of dextran can foster chemical transfers of polysaccharide-Gd^{3+} intermediates to its oxide forms upon addition of ammonium hydroxide. In alkaline environment, polysaccharide-Gd^{3+} complexes are not stable and most likely exhibit transformations from chelated ions, to hydroxide, and finally to oxide. More importantly, this progressive reaction is assisted by the scaffold ability of dextran molecules. One can imagine that in the absence of dextran, Gd^{3+} ions can also be triggered to oxide form in alkaline environment and plus heating, but the resultant could be micro-sized or bulk aggregates. In this study, the participation of dextran can effectively eradicate this phenomenon and incubate separated and ultrasmall-sized nanoparticles.

Figure 1 shows the main physicochemical properties of the prepared GdNPs@Dex. Transmission electron microscopy (TEM) in Figure 1A shows the ultrafine GdNPs@Dex (≈ 3.0 nm) with uniform size distribution without obvious aggregates. It should be noted that this bioinspired synthesis can be easily scaled up to multigram-scale level or higher. The inset in Figure 1A is the lyophilized powder of GdNPs@Dex (12.5 g). The energy dispersive X-ray (EDX) analysis reveals the Gd element in the nanostructure (Figure 1B). The crystal structure of GdNPs@Dex was identified by X-ray diffraction (XRD) analysis. As seen from Figure 1C, the main diffraction peaks in this XRD spectrum are attributed to the crystal structure model of Gd_2O_3 from Powder Diffraction File PDF 12-0797. Relatively low-resolution X-ray photoelectron survey scan, in the binding energy region 0–1200 eV, were recorded for the sample of GdNPs@ Dex, as shown in Figure 1D. The C 1s transition is evident at 284.6 eV associated with the hydrocarbon contamination, which is almost always presented on the samples, used as an energy reference. The valence states of Gd and O components
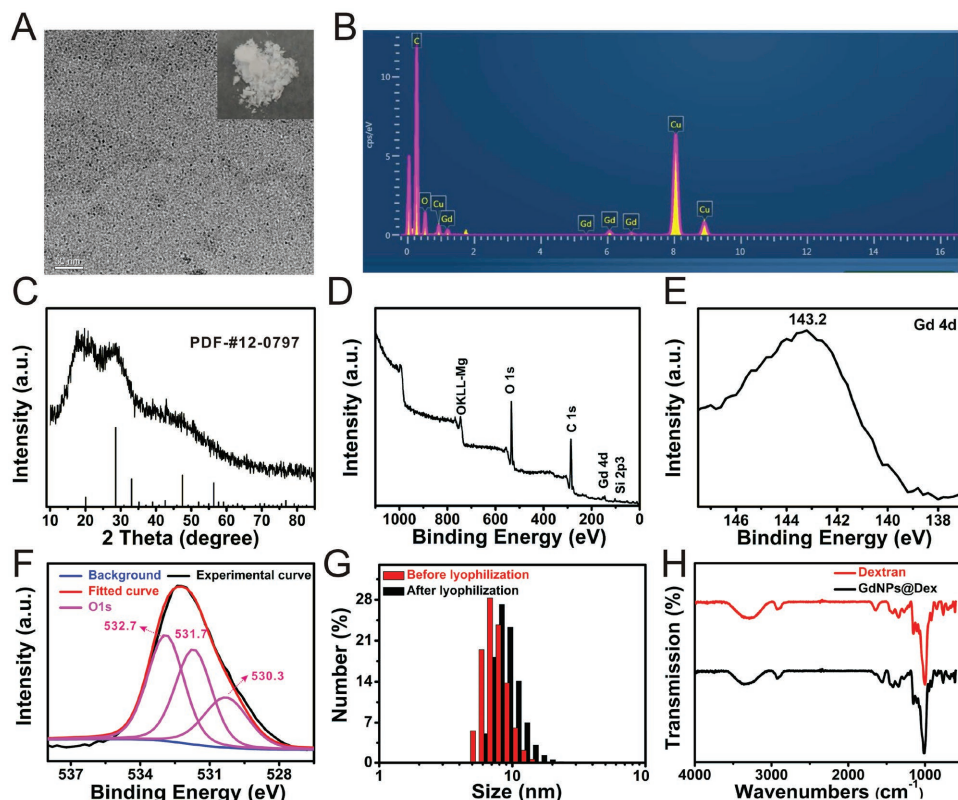
Figure 1. The main physicochemical properties of GdNPs@Dex. A) TEM of GdNPs@Dex (scale bar: 50 nm), inset is the picture of lyophilized powder of GdNPs@Dex; B) EDX spectrum of GdNPs@Dex; C) XRD pattern of GdNPs@Dex; D) a low-resolution XPS spectrum of GdNPs@Dex; E) a high-resolution Gd (4d) spectrum and F) O (1s) spectrum, including experimentally measured curve, background curve, and fitted curve. G) DLS of fresh GdNPs@Dex and redissolved GdNPs@Dex from their lyophilized powder; and H) FTIR spectra of GdNPs@Dex and pure dextran.

ADVANCED
HEALTHCARE
MATERIALS
www.advhealthmat.de

ADVANCED
SCIENCE NEWS
www.advancedsciencenews.com

FULL PAPER

are revealed by the high-resolution X-ray photoelectron spectroscopy (XPS) analysis in Figure 1E,F. It shows the high-resolution Gd spectrum of the GdNPs@Dex nanoparticles in the Gd 4d region. The strong peak at 143.2 eV corresponds to Gd 4d 5/2, which agrees well with the reported value for the Gd_2O_3 phase.[18] High-resolution O 1s spectrum of the GdNPs@Dex nanoparticles is also provided in Figure 1F, showing three peaks at 530.3, 531.7, and 532.7 eV, corresponding to the O in Gd_2O_3 and O in dextran, respectively.[19]

The lyophilized GdNPs@Dex can be easily redissolved in deionized (DI) water or buffers, such as phosphate buffered saline (PBS), borate buffer, etc. The hydrodynamic diameters (HDs) of fresh GdNPs@Dex and redissolved GdNPs@Dex after lyophilization are shown with nearly the same size in Figure 1G. It suggests dextran coating on the Gd-based nanoparticles is effective and conducive to their hydrophilization. Its good water solubility benefits the terminal use and storage; since lyophilized GdNPs@Dex has a longer shelf life compared with their aqueous counterparts and they can be ready for injection just by dissolving them with physiological saline. This successful coating is also supported by the Fourier transform infrared spectroscopy (FTIR) spectra, in which the main characteristic peaks of pure dextran can be found in the FTIR spectrum of GdNPs@Dex (Figure 1H).
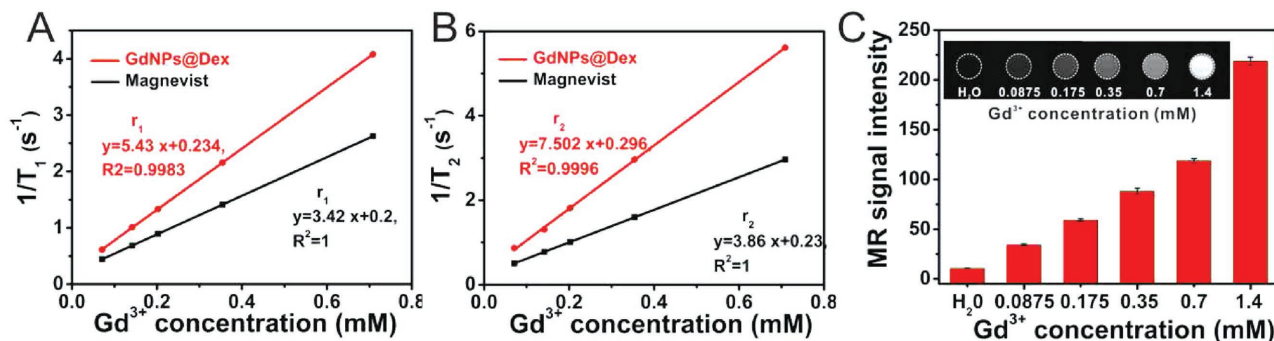
2.2. Relaxivity Study of GdNPs@Dex

To evaluate the capability of GdNPs@Dex as an effective MR contrast agent, their longitudinal (T_1) and transverse (T_2) relaxation times were measured by a 1.41 T NMR analyzer, respectively. The plots of $1/T_1$ and $1/T_2$ versus Gd^{3+} ions concentrations are shown in **Figure 2**A,B. As shown in this figure, GdNPs@Dex exhibits a higher r_1 value of 5.43 s^{-1} × 10^{-3} M^{-1} of Gd^{3+} and r_2 value of 7.502 s^{-1} × 10^{-3} M^{-1} of Gd^{3+}, than those of the commercial Magnevist (Gd-DTPA, $r_1 = 3.42 \times 10^{-3}$ M^{-1} s^{-1}; $r_2 = 3.86 \times 10^{-3}$ M^{-1} s^{-1}) under the same condition. The relaxivity can be improved by nano-sized contrast agents.[20] The increase of r_1 and r_2 values is associated with the confined tumbling of Gd^{3+} in macromolecule of dextran or nanoparticles, resulting in the longer rotational correlation times.[21] The relatively low r_2/r_1 ratio ($r_2/r_1 = 1.38/3$) is beneficial to produce a desired T_1-weighted contrast effect.

For further MRI characterization, T_1-weighted MR images of GdNPs@Dex with various concentrations of Gd^{3+} were obtained. As can be seen from Figure 2C, the MR signals of GdNPs@Dex intensify with increasing Gd^{3+} concentrations. This confirms that GdNPs@Dex behaves as positive contrast agent. The MR signal intensity of GdNPs@Dex is further quantitatively demonstrated. The comparative study on relaxivity suggests superior nano-sized GdNPs@Dex performance over their small Gd^{3+} counterparts, acting as a T_1-enhanced MR contrast agent for biomedical imaging.
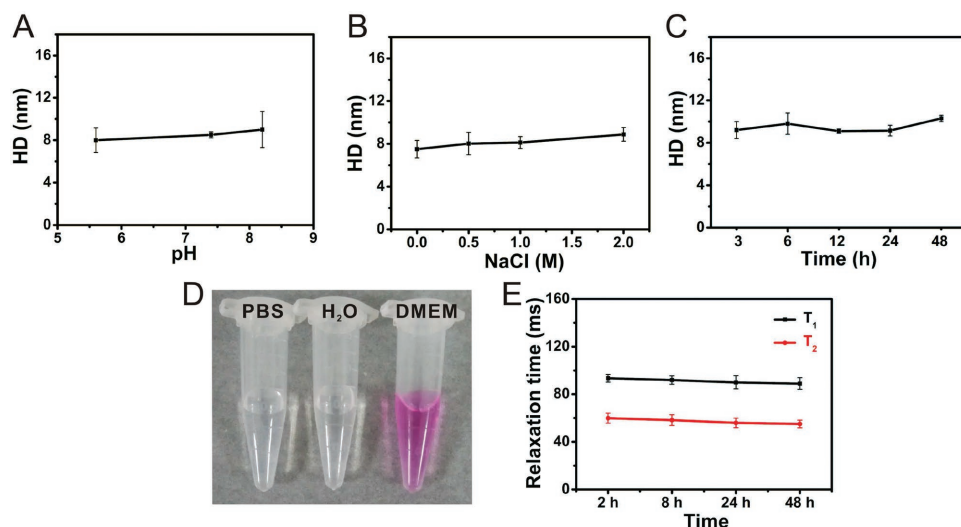
2.3. Stability Study of GdNPs@Dex

The above results show GdNPs@Dex with well-defined structure, good water dispersion capability, sub-10 nm size, and improved relaxivity. These properties are beneficial to their biomedical imaging applications as a MRI contrast agent. Before in vivo imaging, the stability of GdNPs@Dex was further investigated. **Figure 3**A–D shows good colloidal stability of GdNPs@Dex in different buffers with varying pH values and ionic strengths. The HD of GdNPs@Dex has no appreciable difference. The storage time has insignificant effect on HDs of GdNPs@Dex (Figure 3C). The dispersion ability of GdNPs@Dex is observed to be similar in PBS, water, and Dulbecco's modified eagle medium (DMEM) containing 10% fetal bovine serum (FBS) (Figure 3D) without sediments. Particularly, the relaxivity of GdNPs@Dex after different storage time remains stable, shown in Figure 3E, suggesting no Gd^{3+} leaking or nanoparticle aggregating.[6] This prominent stability of GdNPs@Dex is mainly resulted from the dextran-assisted synthesis strategy.

Dextran was used for assisting synthesis of Gd-based nanoparticles in a green chemistry manner, in contrast to the traditional environment-hazardous technical processes. Previously reported synthetic methods involve organic solution and high-temperature heating or reflux processing. Some raw materials with potential toxicity are fed in the reaction. Herein, the dextran-assisted green synthetic route is proved effective and straightforward. The as-prepared GdNPs@Dex exhibits sub-10 nm size and decent relaxivity with good stability. These properties are believed to favor the following in vivo MR imaging.

Figure 2. Relaxivity properties of as-prepared GdNPs@Dex and Magnevist: Plots of A) $1/T_1$ and B) $1/T_2$ versus Gd^{3+} concentration; and C) in vitro T_1-weighted MR images of GdNPs@Dex at varying Gd^{3+} concentrations ranging from 0 to 1.4×10^{-3} M in PBS and their corresponding T_1 signal intensities.

**ADVANCED
SCIENCE NEWS**

www.advancedsciencenews.com

**ADVANCED
HEALTHCARE
MATERIALS**

www.advhealthmat.de

FULL PAPER

Figure 3. Stability study of GdNPs@Dex. A) Colloidal stability at different pH buffers, B) ionic strengths, and C) storage time in PBS; D) the digital photos of GdNPs@Dex dispersed in PBS (1×, pH = 7.4), water, and DMEM containing 10% FBS and 1% PS; E) relaxation time curves of GdNPs@Dex with varying investigated time in PBS.

2.4. Cytotoxicity and Hemolysis Study of GdNPs@Dex

GdNPs@Dex has been identified in this study as an effective T_1-positive MR imaging contrast agent. For in vivo imaging with GdNPs@Dex, biocompatibility is an important factor for clinical applications. The cytotoxicity of GdNPs@Dex was evaluated via standard CCK-8 assays with no obvious cell toxicity. The relative viability can keep up to above 90% even at a high concentration (200 mg L^{-1}) as shown in **Figure 4**A.

Furthermore, the hemolytic behavior of the GdNPs@Dex was investigated at different concentrations by incubating with red blood cells (RBCs), using PBS and deionized water as the negative and positive control, respectively. Inset of Figure 4B shows that negligible red color can be observed in supernatants, which indicate nearly no hemolysis of RBCs occurrence. The calculated hemolysis ratios present unapparent enhancement with the increase of the GdNPs@Dex concentrations (from 6.125 to 200 mg L^{-1}), and the highest hemolysis ratio is

≈0.8%, which is much lower than 5% that for the clinical safety standard.[22] This is indicative that GdNPs@Dex has almost no side effects on blood. This good biocompatibility can be attributed to the dextran encapsulation. It is well known that dextran is a complex branched glucan composed of chains of varying lengths (from 3 to 2000 kDa). It is used medicinally as an antithrombotic (antiplatelet) to reduce blood viscosity, and as a volume expander in hypovolemia.[23] Consequently, GdNPs@Dex is considered to be safe for in vivo applications.

2.5. In Vivo MRI in Tumor-Bearing Mice and Angiogenesis Detection

In vivo MR imaging performance of GdNPs@Dex was investigated on living mice. The solution of GdNPs@Dex was injected via tail vein with the dose of 0.05 mmol Gd kg^{-1} body weight. The T_1-weighted MR images of the mice were recorded at
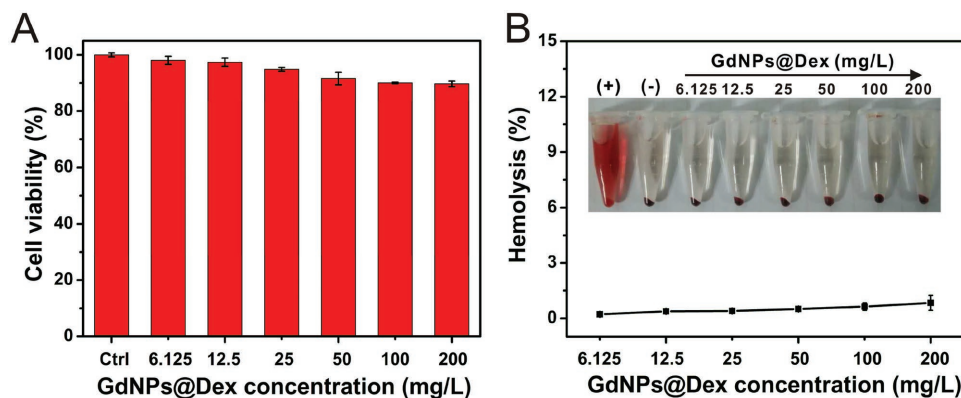
Figure 4. In vitro biocompatibility analysis of GdNPs@Dex: A) Relative viabilities of SK-OV-3 cells incubated with different concentrations (0–200 mg L^{-1}) of GdNPs@Dex. B) Hemolysis assay of GdNPs@Dex after incubation with human red blood cells (RBCs) for 2 h. Inset: The digital picture after centrifugation. PBS and deionized water were used as a negative and positive control, respectively.
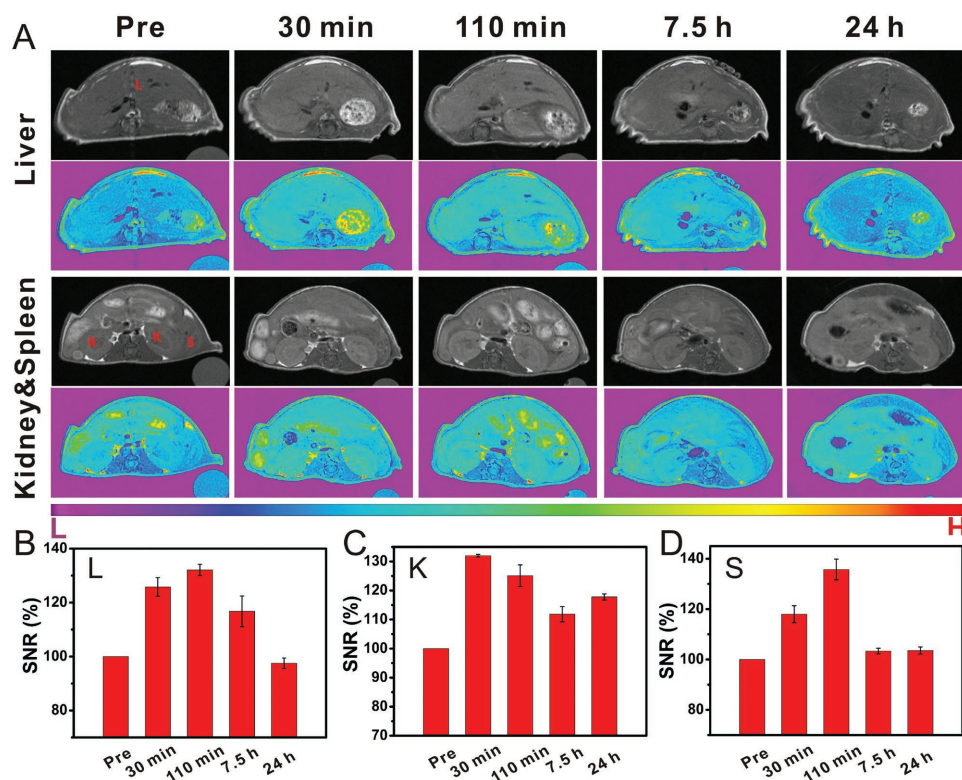
Figure 5. A) T_1-weighted MR images in living mice (TR/TE of 600 ms/6.17 ms) at preinjection and 30 min, 110 min, 7.5 h, and 24 h postinjection of GdNPs@Dex with dosage of 0.05 mmol Gd^{3+} kg^{-1} weight in the regions of the liver (L), kidneys (K), and spleen (S) and quantification of signal-to-noise ratio (SNR) of intensity (post)-to-intensity (pre) contrast in B) liver, C) kidney, and D) spleen at 30 min, 110 min, 7.5 h, and 24 h postinjection of GdNPs@Dex, respectively.

scheduled temporal points pre- and postinjection. As seen from **Figure 5**A, the main organs of mice, liver, kidneys, and spleen, are all significantly enhanced upon injection of GdNPs@Dex at 30 min postinjection. After a period of circulation in blood, the contrast enhancement at these areas is found decreasing, and the signals in liver and spleen at 24 h postinjection decrease to the pre level. The quantified signal-to-noise ratios (SNRs) are further demonstrated in Figure 5B–D. Since organs such as liver and kidney play a vital role in metabolizing nanoparticles, they have been regarded as organs of interest to study the fate of nanoparticles in vivo.[24] The fate of GdNPs@Dex was determined in liver, kidney, and spleen for 24 h in mice. This up-to-down enhancing pattern in these organs is attributed to the uptakes of GdNPs@Dex at first and then metabolized by the body.

It is worth noting that the renal cortexes are clearly visualized in MR imaging by GdNPs@Dex in this study. The MR signal reaches the highest intensity 30 min after injection, indicating a rapid glomerular filtration process, and could be observed for up to at least 110 min. In fact, the enhanced signals at 7.5 and 24 h were also observed. Evidently, GdNPs@Dex is well-secreted by the kidneys; hence, they can serve as an ideal agent for investigating renal anatomy, glomerular physiology, and neoplastic disease process. According to studies on the size-dependent biodistribution of nanoparticles for kidney accumulation, the nanoparticles with a diameter below 20 nm were found in kidneys.[25–27] However, few studies showed significant nanoparticle accumulation in kidneys. In this study, GdNPs@Dex with sub-10 nm in HD exhibits significant contrast enhancement in both kidneys. For kidneys imaging, the contrast agents should be ultrafine to shuttle in glomerulus with a cutoff size of ≈5.5 nm for efficient kidney excretion of nanoparticles.[27,28] The results in this study indicate the escape of GdNPs@Dex from the RES and consequent excretion from the body via the kidney system.

The results of whole body MR imaging show GdNPs@Dex particularly target the kidneys, besides the liver and spleen. To further assess the application potentials in cancer imaging of GdNPs@Dex, in vivo MRI was performed using the mice model with subcutaneous tumor xenografts grown from implanted 4T1 cells. A detectable signal increase in the tumor area can be observed at 24 h postinjection (**Figure 6**). Compared with the MR enhancing kinetics in liver, spleen, and kidneys, it is found that the tumor is gradually enhanced instead of rapidly in the investigated period. It could be ascribed to the difference in density of vessel networks between the metabolic organs of mice and the implanted solid tumors.

Particularly, the boundary between tumor and normal tissue is well-enhanced after GdNPs@Dex administration. The determination of tumor edge is conducive to grading the malignancy of tumors and their treatment schemes.[5,29] In the current study, the boundary is determined by the enhanced angiogenesis around the tumor. And this enhancement is found quite effective, prompt, and persistent, which further discloses the
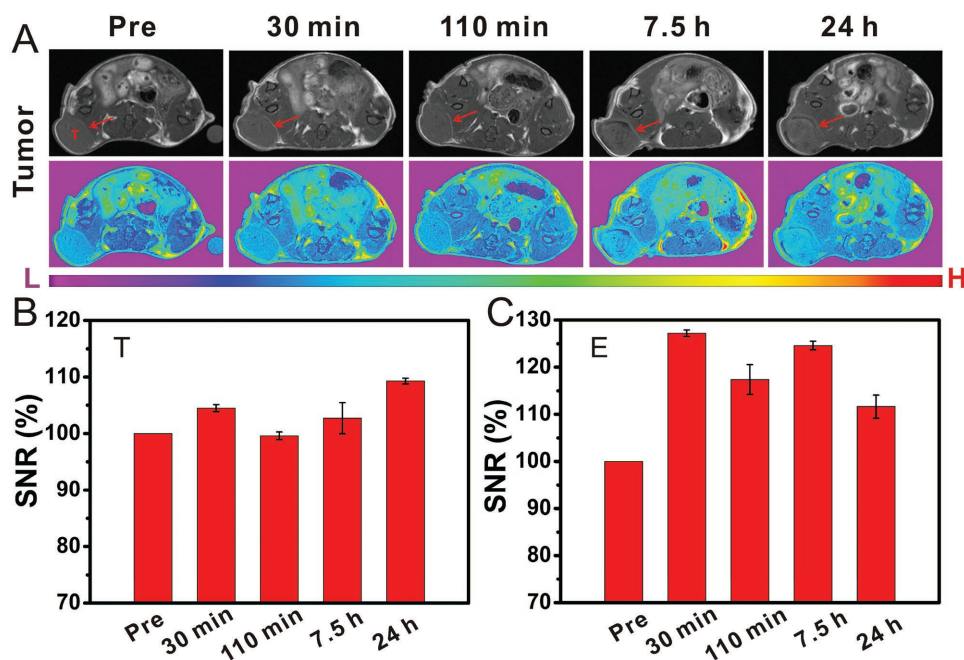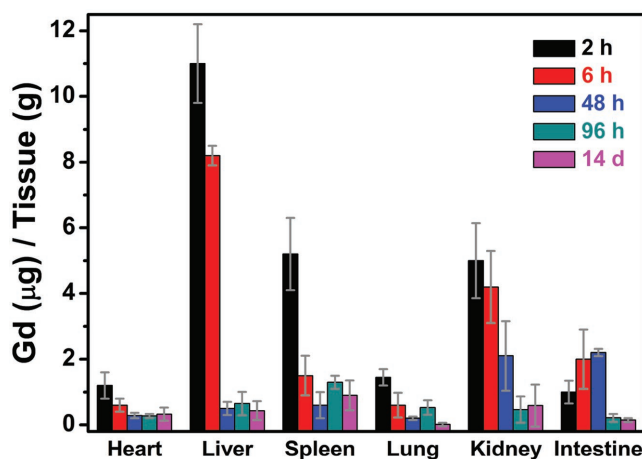
Figure 6. A) Solid tumor and angiogenesis detection in the boundary by T_1-weighted MRI in tumor-bearing mice (TR/TE of 600 ms/6.17 ms) at preinjection and 30 min, 110 min, 7.5 h, and 24 h postinjection of GdNPs@Dex with dosage of 0.05 mmol Gd^{3+} kg^{-1} weight and B) their quantified signal-to-noise ratio (SNR) of intensity (post)-to-intensity (pre) contrast in tumor denoted by T and C) angiogenesis at the edge denoted by E pointed by the arrow at 30 min, 110 min, 7.5 h, and 24 h postinjection of GdNPs@Dex, respectively.

construction of new vascular networks in malignancies, since the growth of solid tumors requires concomitant expansion of vascular networks to maintain the blood supply of oxygen and nutrients.[30] Tumor boundary or edge is not always easily distinguished. It requires the injected nanoparticles reaching the tumor area while being escaped from the RES capture with high efficiency. Generally, large-sized nanoparticles could easily arouse opsonization in blood and further uptake in liver and spleen for an extended period.[24,25] In this fashion, the ultrafine or sub-10 nm nanoparticles can more efficiently target the tumor surroundings, in addition to the kidneys. The imaging in liver and spleen by GdNPs@Dex becomes weakened at 7.5 h postinjection. On the contrary, the kidneys are temporarily intensified, showing RES escape of GdNPs@Dex with decent blood half-life. This advanced imaging property is also verified in the enhanced new blood vessels surrounding the tumor by GdNPs@Dex lasting for at least 7.5 h. The imaging results of tumor and tumor margin in our study are highly identical to the results in a recently published paper.[31] Prospectively, GdNPs@Dex in concert with drugs can be used for vascular-targeting therapies for treatment of malignant disease. The long-time residual in tumor blood vessels of GdNPs@Dex with drugs can disrupt the already formed vessel networks of growing tumors.[30] Interestingly, the MR signals of new blood vessels and the tumor behave differently with the former decrease and the latter increases, suggesting GdNPs@Dex transacting the tumor through the adjacent new vessels. Considering this unique tumor enhancement pattern, it is likely that the intensified periphery of the tumor is a pseudocapsule. Pseudocapsules take place along with solid tumor growing and stimulating the surrounding tissues.[32]

Based on the MRI analyses, GdNPs@Dex is shown to be more resistant to rapid RES uptake compared to other large-sized counterparts. In turn, it is more efficient to reach the cancerous surrounding areas, such as the new blood vessels and tumor tissues. GdNPs@Dex also exhibits longer imaging window time than Magnevist. This imaging strength is attributed to the appropriate HD of GdNPs@Dex and advanced synthetic route. The basic profile descriptions of GdNPs@Dex and the clinically used Magnevist are provided in Table S1 (Supporting Information), including structure format, relaxivity, tumor uptake, MR angiography, and the speed of body clearance.

2.6. Biodistribution and Histological Toxicity Analysis

Time-dependent enhancement pattern reveals that GdNPs@Dex can be metabolized and cleared from body. To further investigate biodistribution of GdNPs@Dex upon administration, dissociated Gd^{3+} ions in main organs were determined via inductively coupled plasma (ICP) analysis technique, in terms of the location, pharmacokinetics, and metabolic behavior of the injected GdNPs@Dex in body. The injected GdNPs@Dex is found at all investigated organs, but with different abundances (**Figure 7**). GdNPs@Dex is primarily captured in the metabolic organs such as liver, kidney, and spleen, and relative lower amount of Gd^{3+} ions are presented in heart and lung. The biokinetics of GdNPs@Dex shown in Figure 6 further shows the time-dependent biodistribution of nanoparticles in every individual organ. Almost all GdNPs@Dex in liver can be found cleared within 48 h. The kidney and intestine are also found

ADVANCED
HEALTHCARE
MATERIALS

www.advhealthmat.de

ADVANCED
SCIENCE NEWS

www.advancedsciencenews.com

FULL PAPER

Figure 7. Biodistribution histogram of GdNPs@Dex in the main organs. Error values were obtained from three parallel tests.

acting as the metabolic organs through the investigated period. This observation agrees well with the findings by MR imaging in vivo. Very few retention of GdNPs@Dex in main organs is mainly attributed to the aggregation of GdNPs@Dex there. Taking the MRI profile and biodistribution pattern into consideration, it is concluded that the clearance of GdNPs@Dex in vivo follows hepatobiliary (HB) and renal hybrid processing.

To investigate the potential toxic side effects induced by GdNPs@Dex, the blood samples of mice ($n = 4$) treated with GdNPs@Dex were collected for blood routine and blood biochemistry assays at 14 days p.i. Other four mice injected of PBS were used as control. For blood routine examination, a series of related standard hematology markers, such as WBC, RBC, HGB, PLT, HCT, MCV, MCH, and MCHC, were analyzed. As displayed in **Figure 8**A–H, all the eight indexes are normal after treatment with GdNPs@Dex. Furthermore, for blood biochemistry assays, we focused on the changes of their liver and kidney function markers, including AST, ALP, ALT, A/G, and BUN.[33] It was found that all these important indexes remain in the normal ranges (Figure 8I–L). These results suggest that intravenous injection of GdNPs@Dex has no noticeable damage to mice. The hepatotoxic and renal toxicity effects even at the dose of 10 mg kg^{-1} are negligible. Furthermore, as GdNPs@Dex is present in all main organs including heart, liver, spleen, lung, kidney, and intestine, the toxicity of the nanoparticles in these organ tissues was assessed by means of the histological changes in the susceptible organs. The GdNPs@Dex injected mice were anesthetized, dissected, and organ tissues were treated for H&E-staining after two week exposure. As seen in Figure 8M, all investigated organ tissues have no obvious histological changes. No observable cell necrosis or inflammatory infiltrate is present in the major organs after administration. This non- or low- toxicity benefits from the green chemistry route and the biosafety raw materials. It can therefore be concluded that GdNPs@Dex is biocompatible in living mice, which is crucial for in vivo biomedical applications.

3. Conclusion

In summary, sub-10 nm GdNPs@Dex is developed at low temperature for MR imaging with several major superior

properties. These include well-defined and stable structure, excellent stability, and high biocompatibility. Enviable relaxivity and rational organ distribution of GdNPs@Dex ensure their high-quality MR imaging of organs interested in this work. In vivo T_1-weighted MRI in tumor-bearing mice shows penetration of GdNPs@Dex into the solid tumor through the surrounding tumor angiogenesis. Particularly, the solid tumor edge can be clearly distinguished with peripheral angiogenesis enhancement around the tumor. This imaging pattern could provide great diagnostic values in differentiating benign and malignant diseases. Furthermore, the synthesis is chemically green, environmentally benign, and methodologically straightforward. All improved properties attribute not only to the unique synthetic route but also the FDA-approved dextran as the matrix. GdNPs@Dex presents great potentials as a positive MR imaging agent for whole body imaging with the particular targeting capabilities for tumors, tumor angiogenesis, and organ interested.

4. Experimental Section

Materials: Reagents were obtained from either Sigma-Aldrich or Alfa and were used directly, unless otherwise noted. DI water (18.2 MΩ cm at 25 °C) was used throughout the entire experiments.

Synthesis of GdNPs@Dex: GdNPs@Dex was synthesized in the solution of reduced dextran. Reduced dextran was prepared according to the reported method with minor modifications.[34] 5 g of dextran (M_W/M_N = 10 000 Da) was dissolved in 100 mL of deionized water at 25 °C, followed by the quick addition of 1 g of sodium borohydride. The mixture was stirred for overnight. The mixture was then purified via dialysis processing with a membrane dialysis bag (MWCO: 12 000 Da) for 48 h (change the water every 8 h). The final product was then lyophilized and stored at 4 °C for further use.

Typically, reduced dextran (30 mg mL^{-1}, 5 mL) and GdCl$_3$•6H$_2$O solution (20 mg mL^{-1}, 2 mL) were mixed in a single-neck flask with magnetically stirring at room temperature for 10 min. Then, 0.5 mL of ammonia was added into above mixture, followed by stirring for another 5 min. Subsequently, the flask was put into water bath at 80 °C stirring continuously for 1 h. In the end, the GdNPs@Dex were obtained by centrifugation (8000 rpm, 15 min) and washed with isopropanol and water three times. The final precipitation was redispersed in 1 mL of borate saline buffer (pH = 8.2) for further characterization and use.

Nanoparticles Characterization: TEM images of GdNPs@Dex were obtained by a Tecnai G2 F20 instrument operated at an acceleration voltage of 200 kV with an EDX detector. Dynamic light scattering (DLS, Nano ZS, Malvern) was used to record the HDs and distribution of GdNPs@Dex. The relaxation rates of GdNPs@Dex and commercial Magnevist were measured on a 1.41 T minispec mq 60 NMR analyzer (Bruker, Germany). The XPS measurements were performed on PHI-5000 CESCA system (Perkin Elmer) with radiation of Al Kα (1486.6 eV) X-ray source. The powder XRD measurement was performed at room temperature by using a Rigaku Ultima III diffractometer equipped with a rotating anode and a Cu Kα radiation source. The FTIR spectra were obtained on a FTIR spectrometer (TENSOR 27, Bruker). The concentrations of the investigated ions were measured by an inductively coupled plasma mass spectrometry (ICP-MS, Hitachi Ltd., Japan).

Relaxivity Characterization and MR Imaging In Vitro: The longitudinal (T_1) and transverse (T_2) relaxation times were determined at a 1.41 T minispec mq 60 NMR analyzer (Bruker, Germany) at 37 °C. The relaxivity values of r_1 and r_2 were obtained by fitting the $1/T_1$ and $1/T_2$ relaxation time (s^{-1}) versus Gd^{3+} ions concentration determined by ICP-MS. T_1-weighted MR imaging of samples was performed in vitro on a GE MR system (3.0 T, Signa HDxt). The specific scanning parameters were set
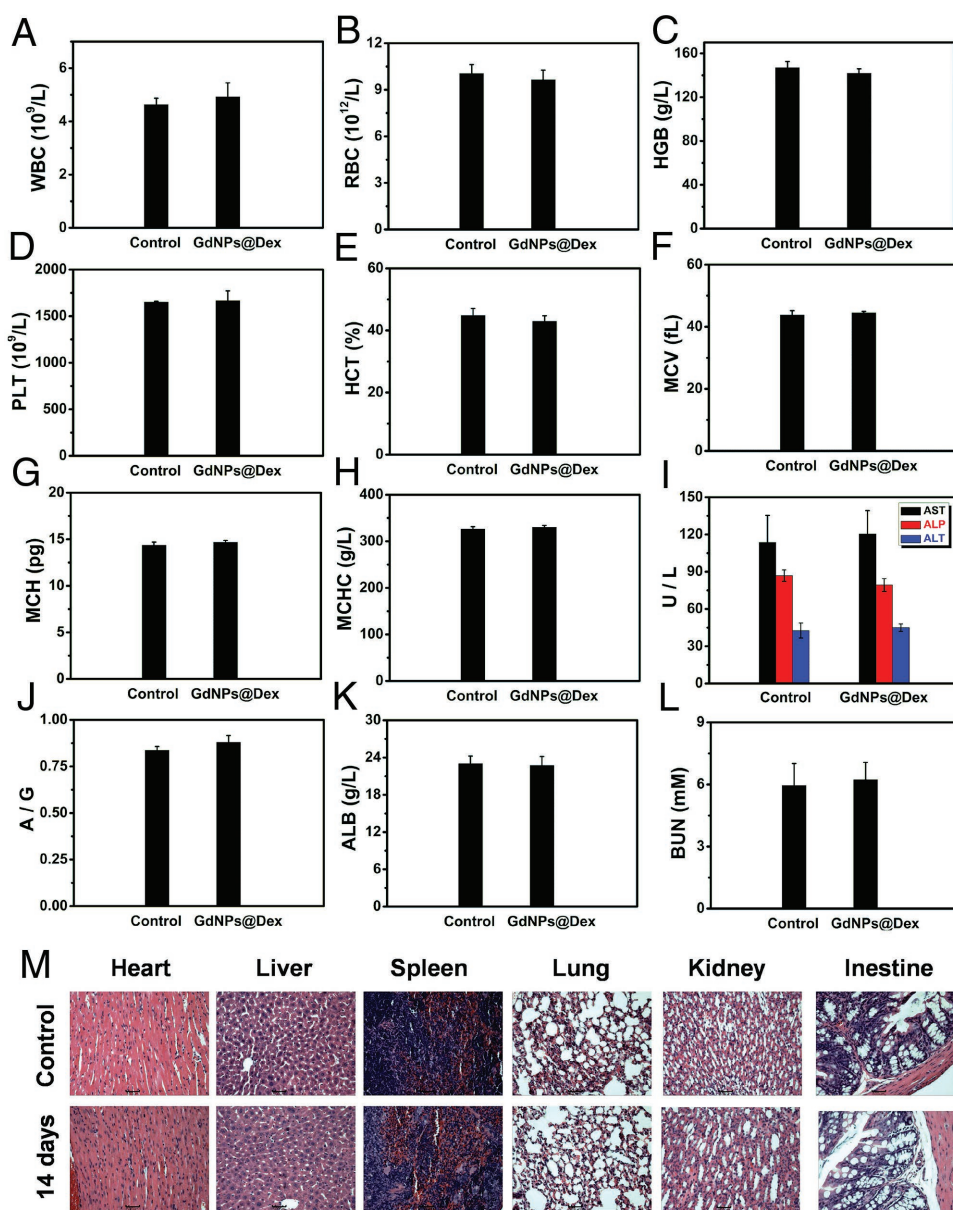
Figure 8. In vivo toxicological evaluation of GdNPs@Dex: Blood routine and blood biochemistry assays before and after intravenous injection with GdNPs@Dex (0.05 mmol Gd kg^{-1} mice): A) white blood cell (WBC) count; B) red blood cell (RBC); C) hemoglobin (HGB) count; D) platelet (PLT) count; E) hematocrit (HCT), F) mean corpuscular volume (MCV), G) mean corpuscular hemoglobin (MCH), and H) mean corpuscular hemoglobin concentration (MCHC). Liver function markers: I) aspartate aminotransferase (AST), alkaline phosphatase (ALP), and alanine aminotransferase (ALT); J) albumin/globulin (A/G) ratio; K) albumin (ALB). Kidney function marker: L) Blood urea nitrogen (BUN). M) Microscopy images of H&E-stained tissue slices harvested from the main organs of the mice including the control group without injection and the experimental group injected with GdNPs@Dex.

as follows: T_1 spin echo sequence, repetition time (TR) = 2000.00 ms, echo time (TE) = 108 ms, matrix = 256 × 192, FOV = 80 mm × 80 mm, FOV phase of 40%, slice width = 2.0 mm, at room temperature.

Colloidal Stability and Relaxivity Stability Studies: The as-prepared GdNPs@Dex was mixed with sodium acetate buffer (0.2 M, pH 5.7), PBS buffer (0.1 M, pH 7.4), and borate buffer (10 × 10^{-3} M, pH 8.2) for evaluating their colloidal stability in different pH environment. And their colloidal stability in different ionic strengths (0, 0.5, 1.0, and 2.0 M) and storage time (3, 6, 12, 24, and 48 h) were also investigated. Moreover, relaxation times (T_1 and T_2) of GdNPs@Dex were recorded after storage in PBS for 2, 8, 24, and 48 h.

Cytotoxicity and Hemolysis Assay: A standard cell counting kit-8 (CCK-8) assay was conducted on ovarian carcinoma cell line (SK-OV-3) to evaluate the in vitro cytotoxicity of GdNPs@Dex. Typically, SK-OV-3 cells (5 × 10^3/well) were seeded into a 96-well plate, and then the cells were incubated in the culture medium for 24 h at 37 °C under 5% CO$_2$ atmosphere. The culture medium was then removed, and cells were incubated with fresh medium containing 100 μL of GdNPs@Dex at varied concentrations (0, 6.125, 12.5, 25, 50, 100, and 200 mg L^{-1}) at 37 °C under 5% CO$_2$ for additional 24 h. 10 μL of CCK8 agentia (5 mg mL^{-1}) was added into the plate replacing the culture medium, and cells were incubated for further 4 h. In the end, the OD450 value (Abs.)

of each well was measured using a multifunction microplate reader (Infinite M200 Pro, Switzerland) for cytotoxicity calculation.

Then, 1.2 mL of GdNPs@Dex solution with varying concentrations (6.125–200 mg L^{-1}) were incubated with 300 µL of human red blood cells (2%) for 2 h followed by centrifugation for 10 min. The obtained supernatants were analyzed by multifunction microplate reader, recording their OD$_{570\,nm}$ values. Deionized water and PBS group were set as the positive and negative control. The hemolysis ratio was calculated using a conventional formula: Hemolysis ratio (%) = (mean value of A (sample, 570 nm) − A (negative, 570 nm))/(mean value of A (positive, 570 nm) − A (negative, 570 nm)).

In Vivo MRI of Tumor-Bearing Mice: All animal experimental procedures were performed in conformity with a standard protocol approved by the Institutional Animal Care and Use Committee of Tongji University. Tumor models were established by injecting subcutaneously 4T1 cells (3×10^6), suspended in 70 µL of PBS, into the right thigh of each female nude mouse (five-week old, body weight: ≈22 g).

In vivo MRI was conducted on a 7.0 T Bruker BioSpec MR imaging system in tumor-bearing mice. The images were acquired before and after intravenous injection at a given time (dosage: 0.05 mmol Gd kg^{-1}) using a T_1-RARE imaging sequence. The detailed MR imaging parameters were set as follows: Field of view (FOV) = 30 mm × 30 mm, repetition time (TR)/echo time (TE) = 600 ms/6.17 ms, number of excitations (NEX) = 3, matrix = 256 × 256, slices = 36, flip angle (FA) = 90°.

In Vivo Biodistribution and Toxicity Analysis: Balb/c mice were intravenously injected with 100 µL of GdNPs@Dex with a same dosage for MRI. Subsequently, mice were sacrificed at varying postinjection time points (2 h, 6 h, 48 h, 96 h, and 14 d), and major organs (heart, liver, spleen, lung, kidney, and intestine) were collected. After digestion with aqua regia (3 mL, V_{HCl}/V_{HNO3} = 3/1) overnight, the solutions were filtered first and then diluted to 10 mL by DI water. Gd^{3+} contents of samples were quantified using ICP-MS technique.

The blood samples and main organ tissues of BALB/c mice (heart, liver, spleen, lung, kidney, and intestine) were harvested after 14 d postinjection via the tail vein (dosage: 10 mg kg^{-1} mice). The whole blood and separated serum samples were sent to Shanghai Research Center for Model Organisms for blood routine and blood biochemistry assays. The organ tissues were fixed with 4% paraformaldehyde followed by being embedded in paraffin, sliced (4 µm), and then stained with hematoxylin and eosin (H&E). All of the obtained samples were observed using an optical microscope (Leica). The mice without injection were used as the control groups.

Supporting Information

Supporting Information is available from the Wiley Online Library or from the author.

Acknowledgements

[1] a) R. L. Ehman, G. E. Wesbey, K. L. Moon, R. D. Williams, M. T. McNamara, W. R. Couet, T. N. Tozer, R. C. Brasch, *Magn. Reson. Imaging* **1985**, *3*, 89; b) D. Weishaupt, F. H. Hetzer, S. G. Ruehm, M. A. Patak, M. Schmidt, J. F. Debatin, *Eur. Radiol.* **2000**, *10*, 1958; c) R. D. Bolskar, A. F. Benedetto, L. O. Husebo, R. E. Price, E. F. Jackson, S. Wallace, L. J. Wilson, J. M. Alford, *J. Am. Chem. Soc.* **2003**, *125*, 5471; d) G. Song, C. Liang, H. Gong, M. Li, X. Zheng, L. Cheng, K. Yang, X. Jiang, Z. Liu, *Adv. Mater.* **2015**, *27*, 6110.

[2] M. Oudkerk, P. E. Sijens, E. J. Van Beek, T. J. Kuijpers, *Invest. Radiol.* **1995**, *30*, 75.

[3] a) W. Zhang, Y. Chen, D. J. Guo, Z. W. Huang, L. Cai, L. He, *Eur. J. Radiol.* **2011**, *79*, 369; b) W. Watcharin, C. Schmithals, T. Pleli, V. Koberle, H. Korkusuz, F. Hubner, O. Waidmann, S. Zeuzem, H. W. Korf, A. Terfort, S. Gelperina, T. J. Vogl, J. Kreuter, A. Piiper, *J. Controlled Release* **2015**, *199*, 63; c) H. Y. Jun, H. H. Yin, S. H. Kim, S. H. Park, H. S. Kim, K. H. Yoon, *Korean J. Radiol.* **2010**, *11*, 449.

[4] a) E. C. Cho, C. Glaus, J. Chen, M. J. Welch, Y. Xia, *Trends Mol. Med.* **2010**, *16*, 561; b) L. Dai, Y. Liu, Z. Wang, F. Guo, D. Shi, B. Zhang, *Mater. Sci. Eng., C* **2014**, *41*, 161.

[5] Y. Li, Z. Li, X. Wang, F. Liu, Y. Cheng, B. Zhang, D. Shi, *Theranostics* **2012**, *2*, 769.

[6] H. Du, J. Yu, D. Guo, W. Yang, J. Wang, B. Zhang, *Langmuir* **2016**, *32*, 1155.

[7] a) W. Guo, W. Yang, Y. Wang, X. Sun, Z. Liu, B. Zhang, J. Chang, X. Chen, *Nano Res.* **2014**, *7*, 1581; b) Y. T. Lim, Y. W. Noh, J. H. Han, Q. Y. Cai, K. H. Yoon, B. H. Chung, *Small* **2008**, *4*, 1640; c) Y. Xiao, R. Xue, T. You, X. Li, F. Pei, *Magn. Reson. Imaging* **2015**, *33*, 822; d) X. Cai, W. Gao, M. Ma, M. Wu, L. Zhang, Y. Zheng, H. Chen, J. Shi, *Adv. Mater.* **2015**, *27*, 6382; e) L. Yang, H. T. T. Duong, S. Laurent, A. Macmillan, R. M. Whan, L. V. Elst, R. N. Muller, J. Hu, A. Lowe, C. Boyer, *Adv. Healthcare Mater.* **2015**, *4*, 148.

[8] X. Xing, B. Zhang, X. Wang, F. Liu, D. Shi, Y. Cheng, *Biomaterials* **2015**, *48*, 16.

[9] W. Yang, W. Guo, X. Gong, B. Zhang, S. Wang, N. Chen, W. Yang, Y. Tu, X. Fang, J. Chang, *ACS Appl. Mater. Interfaces* **2015**, *7*, 18759.

[10] B. Zhang, Q. Li, P. Yin, Y. Rui, Y. Qiu, Y. Wang, D. Shi, *ACS Appl. Mater. Interfaces* **2012**, *4*, 6479.

[11] X. Wang, X. Xing, B. Zhang, F. Liu, Y. Cheng, D. Shi, *Int. J. Nanomed.* **2014**, *9*, 1601.

[12] H. Chen, G. D. Wang, X. Sun, T. Todd, F. Zhang, J. Xie, B. Shen, *Adv. Funct. Mater.* **2016**, *26*, 3973.

[13] a) S. Song, H. Guo, Z. Jiang, Y. Jin, Z. Zhang, K. Sun, H. Dou, *Langmuir* **2014**, *30*, 10557; b) Y. Xu, C. Wu, W. Zhu, C. Xia, D. Wang, H. Zhang, J. Wu, G. Lin, B. Wu, Q. Gong, B. Song, H. Ai, *Biomaterials* **2015**, *58*, 63; c) X. L. Liang, Y. Y. Li, X. D. Li, L. J. Jing, Z. J. Deng, X. L. Yue, C. H. Li, Z. F. Dai, *Adv. Funct. Mater.* **2015**, *25*, 1451.

[14] B. Zhang, H. Jin, Y. Li, B. Chen, S. Liu, D. Shi, *J. Mater. Chem.* **2012**, *22*, 14494.

[15] B. H. Kim, N. Lee, H. Kim, K. An, Y. I. Park, Y. Choi, K. Shin, Y. Lee, S. G. Kwon, H. B. Na, J. G. Park, T. Y. Ahn, Y. W. Kim, W. K. Moon, S. H. Choi, T. Hyeon, *J. Am. Chem. Soc.* **2011**, *133*, 12624.

[16] a) A. T. A. Rahman, P. Majewski, K. Vasilev, *Contrast Media Mol. Imaging* **2013**, *8*, 92; b) J. L. Bridot, A. C. Faure, S. Laurent, C. Riviere, C. Billotey, B. Hiba, M. Janier, V. Josserand, J. L. Coll, L. V. Elst, R. Muller, S. Roux, P. Perriat, O. Tillement, *J. Am. Chem. Soc.* **2007**, *129*, 5076; c) W. Song, W. Di, W. Qin, *Dalton Trans.* **2016**, *45*, 7443.

[17] a) A. Zhang, Y. Tu, S. Qin, Y. Li, J. Zhou, N. Chen, Q. Lu, B. Zhang, *J. Colloid Interface Sci.* **2012**, *372*, 239; b) J. Xie, Y. Zheng, J. Y. Ying, *J. Am. Chem. Soc.* **2009**, *131*, 888.

[18] D. Ferrah, M. El Kazzi, G. Niu, C. Botella, J. Penuelas, Y. Robach, L. Louahadj, R. Bachelet, L. Largeau, G. Saint-Girons, Q. Liu, B. Vilquin, G. Grenet, *J. Cryst. Growth* **2015**, *416*, 118.

[19] S. Yang, H. Gao, Y. Wang, S. Xin, Y. He, Y. Wang, W. Zeng, *Mater. Res. Bull.* **2013**, *48*, 37.

**ADVANCED
SCIENCE NEWS**

www.advancedsciencenews.com

**ADVANCED
HEALTHCARE
MATERIALS**

www.advhealthmat.de

FULL PAPER

[20] H. Wu, H. H. Wang, H. Liao, Y. Lv, X. J. Song, X. J. Ma, M. Q. Tan, *Adv. Healthcare Mater.* **2016**, *5*, 311.

[21] a) Z. Zhang, M. T. Greenfield, M. Spiller, T. J. McMurry, R. B. Lauffer, P. Caravan, *Angew. Chem., Int. Ed. Engl.* **2005**, *44*, 6766; b) B. B. Zhang, X. Q. Gong, Z. Q. Li, F. F. Guo, S. Y. Cai, J. L. Kong, Q. H. Yang, H. Ma, J. Chang, D. L. Shi, *Chem. J. Chin. Univ.* **2010**, *31*, 982.

[22] L. Li, C. Chen, H. Liu, C. Fu, L. Tan, S. Wang, S. Fu, X. Liu, X. Meng, H. Liu, *Adv. Funct. Mater.* **2016**, *26*, 4252.

[23] L.-O. Lamke, S.-O. Liljedahl, *Resuscitation* **1976**, *5*, 93.

[24] W.-S. Cho, M. Cho, J. Jeong, M. Choi, B. S. Han, H.-S. Shin, J. Hong, B. H. Chung, J. Jeong, M.-H. Cho, *Toxicol. Appl. Pharmacol.* **2010**, *245*, 116.

[25] W. H. De Jong, W. I. Hagens, P. Krystek, M. C. Burger, A. J. A. M. Sips, R. E. Geertsma, *Biomaterials* **2008**, *29*, 1912.

[26] R. Kumar, I. Roy, T. Y. Ohulchanskky, L. A. Vathy, E. J. Bergey, M. Sajjad, P. N. Prasad, *ACS Nano* **2010**, *4*, 699.

[27] C. Sun, H. Yang, Y. Yuan, X. Tian, L. Wang, Y. Guo, L. Xu, J. Lei, N. Gao, G. J. Anderson, X. J. Liang, C. Chen, Y. Zhao, G. Nie, *J. Am. Chem. Soc.* **2011**, *133*, 8617.

[28] M. Longmire, P. L. Choyke, H. Kobayashi, *Nanomedicine* **2008**, *3*, 703.

[29] a) Q. T. Nguyen, E. S. Olson, T. A. Aguilera, T. Jiang, M. Scadeng, L. G. Ellies, R. Y. Tsien, *Proc. Natl. Acad. Sci. USA* **2010**, *107*, 4317; b) Q. T. Nguyen, R. Y. Tsien, *Nat. Rev. Cancer* **2013**, *13*, 653.

[30] D. W. Siemann, D. J. Chaplin, M. R. Horsman, *Cancer* **2004**, *100*, 2491.

[31] J. Wang, J. Liu, Y. Liu, L. Wang, M. Cao, Y. Ji, X. Wu, Y. Xu, B. Bai, Q. Miao, *Adv. Mater.* **2016**, *28*, 8950.

[32] L. Grazioli, L. Olivetti, C. Fugazzola, A. Benetti, C. Stanga, E. Dettori, C. Gallo, L. Matricardi, A. Giacobbe, A. Chiesa, *Eur. Radiol.* **1999**, *9*, 62.

[33] a) X. Zhong, K. Yang, Z. Dong, X. Yi, Y. Wang, C. Ge, Y. Zhao, Z. Liu, *Adv. Funct. Mater.* **2015**, *25*, 7327; b) X. Yi, K. Yang, C. Liang, X. Zhong, P. Ning, G. Song, D. Wang, C. Ge, C. Chen, Z. Chai, *Adv. Funct. Mater.* **2015**, *25*, 4689.

[34] K. G. Paul, T. B. Frigo, J. Y. Groman, E. V. Groman, *Bioconjugate Chem.* **2004**, *15*, 394.